Theoretical, CFD Simulation and Experimental Study to Predict the Flowrate Across a Square Edge Broad Crested Weir Depending on the End Depth as a Control Section

Sadiq S. Muhsun, Sanaa A. Talab Al-Osmy, Shaymaa Abdul Muttaled Al-Hashimi and Zainab T. Al-Sharify

Abstract A rectangular broad crested weir is the one mostly used in hydraulic structures for measuring flow rates in open channels and rivers. This study is focused on finding the suitable position of the depth above the weir as control section for estimating the flow rate while avoiding the troubles of approach velocity. It was predicted that the end edge of the weir, as a control section, relates to the critical depth (Y_c) as a function of the end depth (Y_e). To determine the relationship between these, experimental tests were achieved with ten different values of the longitudinal slope. Statistical regression analysis indicated the relationship between Y_c and Y_e as about 1.522. Consequently, a new flow rate formula was derived to estimate the flow over the weir and provided a good agreement with the experimental tests. A 3D ANSYS FLUENT Ver. V.16.1 CFD model was also applied to simulate the problem and verify the equation. The water volume fraction and the stream flow pattern were taken into the consideration. The model was able to simulate the problem with a good accuracy for all cases with a percentage error less than 10% when compared to experimental results. Thus indicating that CFD models could be relied upon for describing complex flows.

Keywords Broad weir · CFD · Critical depth · ANSYS · Flow rate

S. S. Muhsun (✉) · S. A. Talab Al-Osmy · S. A. M. Al-Hashimi
Department of Water Resources, College of Engineering, University of Mustansiriya, P.O. Box 14150 Bab-al-Mu'adhem, Baghdad, Iraq

Z. T. Al-Sharify
Department of Environmental Engineering, College of Engineering, University of Mustansiriya, P.O. Box 14150 Bab-al-Mu'adhem, Baghdad, Iraq

Z. T. Al-Sharify
Department of Chemical Engineering, University of Birmingham, Edgbaston, B15 2TT Birmingham, UK

F. Mohamed Nazri (ed.), *Proceedings of AICCE'19*, Lecture Notes in Civil Engineering 53, https://doi.org/10.1007/978-3-030-32816-0_2

1 Introduction

Weirs are a small overflow-type dams commonly used to raise the level of a river or stream and cause a large change of water level behind them. It is likely that the flow discharge exceeds the capacity of a channel or river and, thus, a control structure such as side weirs should be employed to protect the system against overflow [1]. One of the most widely used hydraulic structures for measuring flow rates in open channels and rivers is a rectangular broad crested weir [2]. Weirs are generally divided into two groups, namely, sharp-crested weirs and weirs of finite crest length. The second group has been further subdivided into three groups, namely, long-crested, broad crested and narrow-crested weirs, depending on the value of the h/L, where h is the head over the weir measured some distance upstream of the weir where the water surface is essentially horizontal while L is the crest length in the longitudinal direction [1]. Farzin et al. [3], performed a series of laboratory experiments in order to investigate the effects of width of the lower weir crest and step height of broad-crested weirs with rectangular compound cross section on the values of the discharge coefficient (C_d) and the approach velocity coefficient. For this purpose, 15 different models with a wide range of discharges were tested. The results showed that a discontinuity occurs in head-discharge ratings because the section width suddenly changes shape, experiencing a break in slope when the flow enters the outer section. Values of C_d obtained from the experiments on compound broad-crested weirs are lower than those of a broad crested weir with a rectangular cross section because of it's contraction effects. Maghsoodi et al. [4], used the Computational Fluid Dynamics (CFD) to simulate free surface flow over Submerged Weirs. A (Fluent) numerical model was used to numerical modeling. The model solved the fully three-dimensional, Reynolds-averaged Navier–Stokes (RANS) equation to predict flow near the structure where three dimensional flows were dominant. They simulated the problem using the volume of fluid (VOF) method with standard $k - \varepsilon$ equations. The computed results using numerical model on compressed mesh systems were found in good agreement with measured experimental data. Studying the hydraulic characteristics of flow over rectangular broad-crested weirs with varying upstream slopes experimentally was done by Ehsan et al. [2]. A series of laboratory experiments was performed to investigate the effects of changing upstream slopes from 90° to 75°, 60°, 45°, 30°, 22.5°, 15°, and 10° on the flow surface pattern, discharge coefficient values, approach velocity profile and flow separation zone. In addition, a new mathematical relationship for water surface profile and a new correction factor to estimate discharge coefficient over weirs with various upstream slopes were introduced. The results showed decreasing upstream slopes from 90° to 10° leading to increasing discharge coefficient values and dissipation of the separation zone. The Flow over a Triangular Broad-Crested Weir was studied by Seyed et al. [5]. In their study, basic experiments were conducted on a triangular broad-crested weir. Also, Computational Fluid Dynamics (CFD) model together with laboratory model were used to determine the free-surface profile of rectangular broad-crested weir.

Simulations were performed using the volume of fluid (VOF) and turbulence model of the RNG k − ε to find the water level profile and results are compared with several experimental data. Samadi and Arvanaghi [6] simulated the three-dimensional flow on contracted compound arched rectangular sharp crested weirs using FLUENT software. VOF method was used for multiphase flow simulation while they used RNG $k - \varepsilon$ turbulence model for simulation of turbulent flow. The result of the numerical model was compared with experimental data. The results indicated that FLUENT simulate flow on contracted compound arched rectangular sharp crested weirs with a high accuracy and the software could be efficiently used for determine the discharge coefficient on contracted compound weirs. Shaker et al. [7] investigated the effects of surface roughness sizes on the discharge coefficient for a broad crested weir. For this purpose, three models having different lengths of broad crested weirs were tested in a horizontal flume. In each model, the surface was roughed four times. Experimental results of all models showed that the logical negative effect of roughness increased on the discharge (Q) for different values of length. The performance of broad crested weir improved with decrease ratio of roughness to the weir height (Ks/P) and with the increase of the total Head to the Length (H/L). An empirical equation was obtained to estimate the variation of discharge coefficient C_d. Seyed and Hossein [8] conducted several experiments on rectangular broad-crested weirs with different geometry under Subcritical Flow Conditions. It was found that the discharge coefficient of a rectangular broad-crested weir is related to the upstream total head above the crest, length of weir and Channel breadth. A reliable equation for calculating the discharge coefficient of rectangular broad-crested weirs in subcritical flow conditions is presented. Good agreements between the measured values and that of predictive equation are obtained. Experimental study and CFD mathematical based on Comsol ver. 4.2 was prepared by Sadiq [9] to study the effect of the longitudinal slope on the variation of discharge coefficient of the weir and spillway. It was shown that the longitudinal slope has a great significant effect on the values of the discharge coefficient for both the weir and the spillway. The Discharge Coefficient of Broad-Crested weir in natural channels was studied by Ahmed [10]. The Hydrologic Engineering Center-River Analysis System (HEC-RAS) step back water technique was used to calculate water surface profiles for natural channels that are likely used for storm water drainage. The results indicate that the weir coefficient can be expressed as a function of weir height and channel cross-section area. The experimental and numerical simulation of flow over broad crested weir and stepped weir using different turbulence models was studied by Al-Hashimi et al. [11]. In their study, FLUENT software as a type of Computational Fluid Dynamics (CFD) model was represented as a numerical model to simulate flow over weirs which was governed by Reynold averaged Navier Stoke equation. Their model results were compared with the experimental results. The structured mesh with high concentration near the wall regions was employed in the numerical model. The volume of fluid (VOF) method with four turbulence models which were (Standard k − ε, RNG k − ε, Realizable k − ε and Standard k − ω) was applied for the estimation of the free surface profile. Their study results showed that the

flow over weirs was turbulent and the free surface characteristics were complex and often difficult to be predicted. Also, the comparison of water surface profile between experimental value and numerical results obtained from the turbulent models showed that the standard k − ε model has the best similarity and standard k − ω model has the minimum similarity with experimental value. Sadiq and Al-Sharify [12] studied the effect of the longitudinal slope. So on the depth over the OGEE spillway crest Y_{og} and its relationship with the critical depth Y_c and flow rate. A laboratory experiment was conducted to determine the relationship between the two depths by considering ten different values of the slope ranging from 0 to 0.02. Statistical regression analysis indicates that the relationship between Y_c and Y_{og} is about 1.2 and has insignificant change with the changes of the value of the longitudinal slope S_o. Using this relationship, a new flow rate formula over an OGEE spillway was obtained with a very good agreement comparing with the experimental results and CFD simulated model. Thulfikar et al. [13] used flume experiments and a Computational Fluid Dynamic (CFD) model to study flow properties and scour around four new shapes of submerged weir: inclined sharp crested weirs with 30° and 120° slopes, respectively. It was shown that for local scour, the results of the CFD simulation was a statistically significant difference from that of the flume experiments for both the sharp crested weir and the inclined weir with a 120° angle.

2 Theoretical Considerations

Discharge calculations for broad crested weir can be given by the following equation depending on the continuity principle and the critical depth [14–20]:

$$Q = C\sqrt{g}BY_c^{3/2} \tag{1}$$

where Q is the flow rate in m^3/s, Y_c is the critical depth (m), b is the breadth of the weir in m, g is the acceleration due to gravity m/s^2 and C is the discharge coefficient Based on Bernoulli equation, the flow equation of the weir, which shown in Fig. 1,

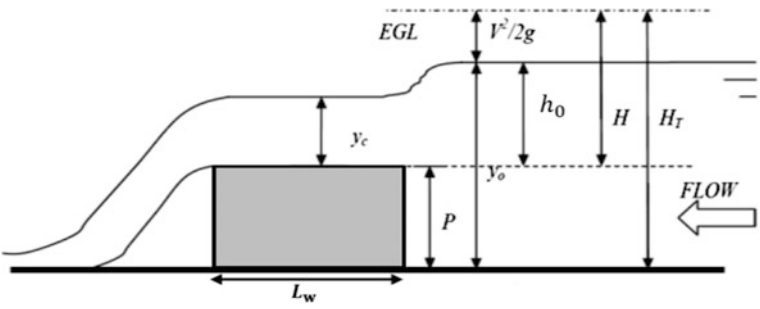

Fig. 1 Flow across right edge broad crested weir

could express the following relationship in Eq. (2) between weir discharge and the head over the crest [21].

$$Q = C\frac{2}{3}\sqrt{\frac{2}{3}gB}(H)^{3/2} \tag{2}$$

In real fluid, the head above crest of the weir is given by Eq. (3),

$$\boldsymbol{H = h_o + \frac{Q^2}{2gB^2(y_o - P)^2}} \tag{3}$$

Usually, the approach velocity ($V^2/2g$) is very small, so that h_o equal to H in Eqs. (2) and (3) becomes as Eq. (4);

$$\boldsymbol{Q = C\frac{2}{3}\sqrt{\frac{2}{3}gB}(h_o)^{3/2}} \tag{4}$$

where H is the head above weir crest including the approach velocity (m) and h_o is the head above weir crest without approach velocity (m). Other variable as earlier defined.

The problem with Eq. (4) is how to satisfy the position of h_o and the difficulty of measuring it. Therefore, it is more easy and suitable to depend on Eq. (1) for flow rate estimation. But in this case the problem again is how to satisfy the position where the critical depth Y_c take places. Therefore, in this work it is decided to consider the end edge of the weir as a control section with a function of $Y_c = f(Y_e)$. This is because in this section the depth is very clear and specified and it is a very easy to measure it. The function $Y_c = f(Y_e)$ represents the relationship between the critical depth and the depth at the end edge of the weir (Y_e).

$$Y_c = f(Y_e) \tag{5}$$

Considering Eq. (5), Eq. (1) will take the following form.

$$Q = C\sqrt{g}B[f(Y_e)]^{3/2} \tag{6}$$

The issue now is how to find this function or the relationship. The best way is to estimate it practically in the laboratory. Therefore, all the efforts were devoted in the hydraulic lab to achieve that.

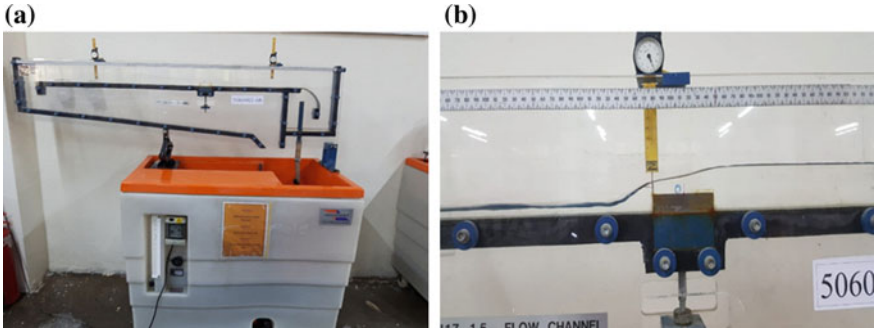

Fig. 2 Photograph of the **a** hydraulic bench and flume, **b** Vernier and sharp edge broad crested weir

3 Experimental Work

The experimental work was conducted in the Hydraulic Engineering Laboratory of Mustansiriya University, Baghdad-Iraq. The devices used and the method employed are explained below. The photographic views of the experimental set-up and the apparatus used in this study are shown in Fig. 2a and b. The set-up consists of a main open channel flume of 1.5 m length and 0.051 m width fitted above an Armfield, F1–10 Hydraulic Bench. For the right edge broad crested weir, a steel model of 1.9 cm height was used in addition to Vernier Calipers to measure the depth at the end of the weir. The volumetric flow rate was estimated with the help of the F1–10 Hydraulic Bench and a stop watch. CFD simulated model was also prepared and operated according to the principles of computational fluid dynamics technique to compare the experimental results and verified.

3.1 Experimental Program

The experimental measurements were made taking the bed slope of the flume to a different ten values of 0–0.0495. The initial flow rate Q was set to a low value and the depth (Y_e) at the end of the weir was measured. For each flow rate Q, the corresponding critical depth is calculated using Eq. (7).

$$Y_c = \sqrt[3]{\frac{Q_a^2}{B^2 * g}} \tag{7}$$

where Q_a is the actual flow rate (m^3/s) and B is the width of the flume (0.051 m).

To complete one test, the flow rate was increased in suitable increments to achieve approximately 8 runs for each value of the longitudinal slope S_o. Then, the

bed slope S_o was increased and the above steps were repeated again. Through this procedure, ten values of the longitudinal slope were considered between 0 and 0.0495.

4 Results and Discussions

Table 1 represents the results of the first test at the longitudinal slope of $S_o = 0$ for while Fig. 3 shows the relationship between the actual depth at the end of the weir (Y_e) and theoretical critical depth (Y_c) calculated from the actual flow rate using Eq. (7). According to the figure, the relationship between the depths could be strongly considered as linear in nature. Therefore, the relationship may be expressed in the following form:

$$Y_c = k\, Y_e \tag{8}$$

Table 1 Results of the first experimental test with $S_o = 0$

Run	Volume (L)	T (s)	Q (L/s)	Y_e (mm)	$Y_c = \sqrt[3]{\frac{Q_a^2}{B^2 * g}}$ (mm)
1	5	88.50	0.0565	2.90	5.00
2	10	89.19	0.1121	4.80	7.90
3	15	84.30	0.1779	7.00	10.75
4	15	66.85	0.2244	8.30	12.54
5	20	71.36	0.2803	9.30	14.55
6	25	75.87	0.3295	11.20	16.20
7	30	70.28	0.4269	13.70	19.26
8	35	71.50	0.4895	15.20	21.10

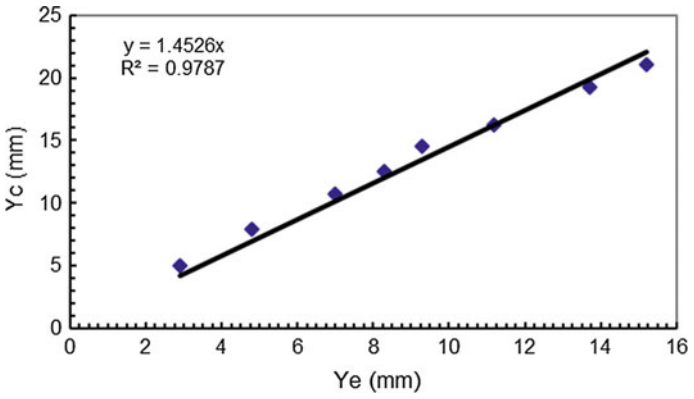

Fig. 3 Y_c versus Y_{ce} relationships for first test of $S_o = 0$

Table 2 Variation of k-values with slope and mean

No.	Slope	*K, for* S_o	*k*, Eq. (9)	Per. error from mean
1	0	1.4526	1.4561	4.3
2	0.0063	1.4811	1.4709	3.4
3	0.0225	1.4824	1.5095	0.8
4	0.028	1.5465	1.5226	0.02
5	0.0289	1.5043	1.5247	0.16
7	0.0326	1.5236	1.5335	0.7
6	0.0333	1.543	1.5351	0.8
8	0.035	1.5817	1.5392	1.1
9	0.0425	1.5279	1.5570	2.28
10	0.0495	1.5792	1.5736	3.37
Mean		1.522		

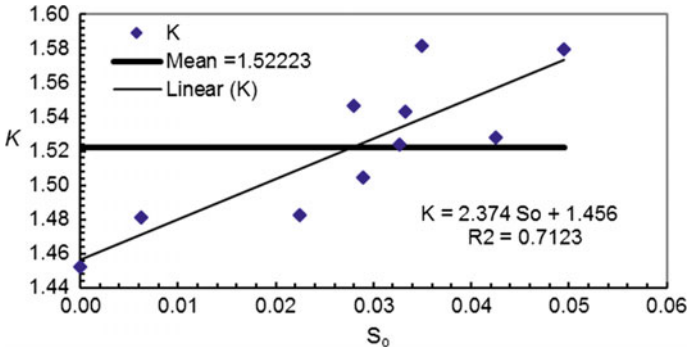

Fig. 4 The effect of S_o on the relationship between Y_c and Y_e

where k is a constant value represents the gradient of the best fit line of the linear relationship estimated using the statistical method of the linear regression analysis [22].

Table 2 explains the results of the constant k for the other ten experimental tests of S_o from 0 to 0.0495. Figure 4 shows the variation of the constant k versus the longitudinal slope S_o, which could de represented as:

$$k = 1.456 + 2.374 S_o \tag{9}$$

As Table 2 shown, the values of the constant k calculated from Eq. (9) has insignificant change from the overall mean value of the constant k. therefore, the relationship between the (Y_c and Y_e) or the required function $Y_c = f(Y_e)$ could be considered depending on the mean value of the constant k. In other words:

$$Y_c = 1.522Y_e \tag{10}$$

4.1 Flow Rate Estimation

As mentioned earlier, the flow rate over the weir can be estimated using Eq. (6) in term of the function $Y_c = f(Y_e)$. Considering Eq. (10) as the relationship between the (Y_c and Y_e), Eq. (6) will take the following form:

$$Q = \sqrt{g}B(1.522Y_e)^{3/2} \tag{11}$$

where Q is the flow rate in m^3/s, g is the gravity acceleration 9.81 m/s^2 and B is the weir or channel width in m.

The relationship between the (Y_c and Y_e) or the function Y_c = f (Y_e) of Eq. (10) is already taking in a count all losses of flow since it is an experimental relationship. Therefore, the dimensionless coefficient of discharge C was ignored from the formula of Eq. (11) since it is included implicitly in Eq. (10).

Figure 5 shows the verification of Eq. (11) corresponding to the actual flow rate for the all the ten experimental tests. While Fig. 6 explains the verification of the formula for each test individually. As the figures show, the formula indicates an excellent verification with the all cases. Furthermore the formula was statistically analyzed using some of standard error indexes in order to investigate the confidence of the formula in estimation of the flow rate as indicated in Table 3. As Table 3 shows, the formula indicates an excellent accuracy giving a very good confidence for the purpose of flow rate estimation.

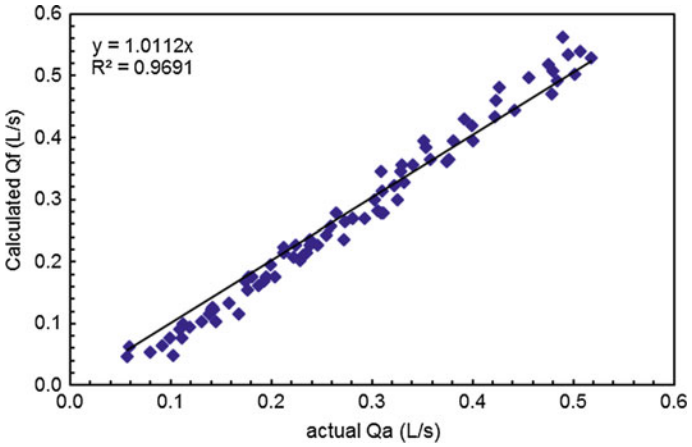

Fig. 5 Over all verification of the new formula of Eq. (11)

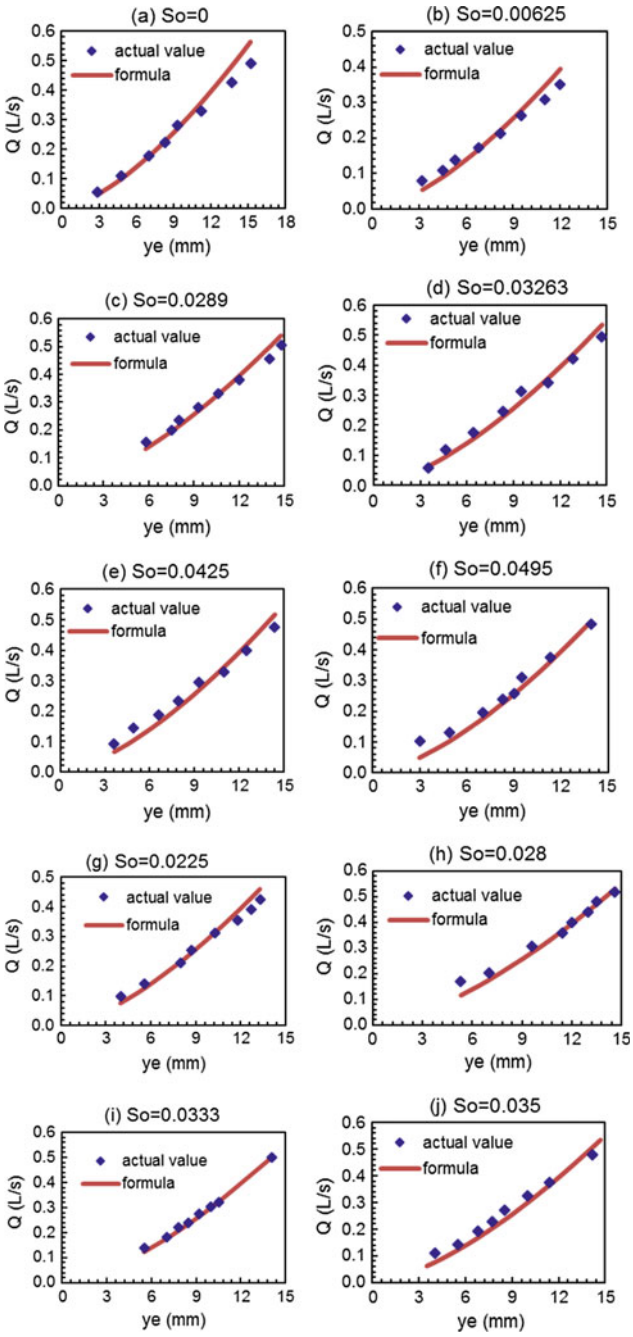

Fig. 6 Individual verification of the new formula, Eq. (11)

Table 3 Statistical analysis test for the new formula of Eq. (11)

No.	Slope	RMSE	MSE	MAE	MAPE %	RSE
1	0	0.031	0.0012	0.024	8.74	0.058
2	0.0063	0.025	0.0006	0.022	12.85	0.067
3	0.0225	0.024	0.0006	0.020	8.53	0.033
4	0.028	0.023	0.0005	0.018	7.58	0.027
5	0.0289	0.023	0.0005	0.019	6.48	0.034
6	0.0326	0.024	0.0006	0.022	9.23	0.026
7	0.0333	0.009	0.0007	0.007	3.534	0.006
8	0.035	0.027	0.0007	0.026	12.593	0.042
9	0.0425	0.029	0.0008	0.008	13.603	0.057
10	0.0495	0.026	0.0007	0.021	13.042	0.046

where

$$RMSE = \sqrt{\frac{1}{n}\sum_{i=1}^{n} e_i^2} \tag{12}$$

$$MSE = \frac{1}{n}\sum_{i=1}^{n} e_i^2 \tag{13}$$

$$MAE = \frac{1}{n}\sum_{i=1}^{n} |e_i| \tag{14}$$

$$MAPE = \frac{100\%}{n}\sum_{i=1}^{n} \left|\frac{e_i}{Q_a}\right| \tag{15}$$

$$RSE = \frac{\sum_{i=1}^{n} e_i^2}{\sum_{i=1}^{n} (Q_a - \bar{Q}_a)^2} \tag{16}$$

RMSE is the Root mean squared error. MSE is the Mean squared error. MAE is the Mean absolute error. MAPE is the Mean absolute percentage error. n is the total observed number. e is the error (Q actual − Q formula = $Q_a - Q_f$), $\overline{Q_a}$ is the mean of Q_a.

4.2 CFD Simulated Model

Recently authors strongly state that the computational fluid dynamics (CFD) techniques considered as a very powerful tool to simulate different fluid

dynamic problems [11, 12, 23–25]. In this work ANSYS FLUENT Ver. V.16.1 was used to simulate the flow over the weir.

4.2.1 Governing Equations

The following equations are the basic govern equations describe the problem:

Continuity equation

$$\frac{\partial \rho}{\partial t} + \frac{\partial (\rho u)}{\partial x} + \frac{\partial (\rho v)}{\partial y} + \frac{\partial (\rho w)}{\partial z} = 0 \tag{17}$$

Momentum equation (assumed a homogeneous fluid and an incompressible flow):

$$\rho\left(\frac{\partial u}{\partial t} + u\frac{\partial u}{\partial x} + v\frac{\partial u}{\partial y} + w\frac{\partial u}{\partial z}\right) = -\frac{\partial p}{\partial x} + \rho g_x + \mu\left(\frac{\partial^2 u}{\partial x^2} + \frac{\partial^2 u}{\partial y^2} + \frac{\partial^2 u}{\partial z^2}\right) \tag{18}$$

$$\rho\left(\frac{\partial v}{\partial t} + u\frac{\partial v}{\partial x} + v\frac{\partial v}{\partial y} + w\frac{\partial v}{\partial z}\right) = -\frac{\partial p}{\partial y} + \rho g_y + \mu\left(\frac{\partial^2 v}{\partial x^2} + \frac{\partial^2 v}{\partial y^2} + \frac{\partial^2 v}{\partial z^2}\right) \tag{19}$$

$$\rho\left(\frac{\partial w}{\partial t} + u\frac{\partial w}{\partial x} + v\frac{\partial w}{\partial y} + w\frac{\partial w}{\partial z}\right) = -\frac{\partial p}{\partial z} + \rho g_z + \mu\left(\frac{\partial^2 w}{\partial x^2} + \frac{\partial^2 w}{\partial y^2} + \frac{\partial^2 w}{\partial z^2}\right) \tag{20}$$

k-equation

$$\begin{aligned}\frac{\partial (\rho k)}{\partial t} + \frac{\partial (\rho u k)}{\partial x} + \frac{\partial (\rho v k)}{\partial y} + \frac{\partial (\rho w k)}{\partial w} = {} & \frac{\partial}{\partial x}\left[\left(\mu + \frac{\mu_t}{\sigma_k}\right)\left(\frac{\partial k}{\partial x} + \frac{\partial k}{\partial y} + \frac{\partial k}{\partial z}\right)\right] \\ & + \frac{\partial}{\partial y}\left[\left(\mu + \frac{\mu_t}{\sigma_k}\right)\left(\frac{\partial k}{\partial x} + \frac{\partial k}{\partial y} + \frac{\partial k}{\partial z}\right)\right] \\ & + \frac{\partial}{\partial z}\left[\left(\mu + \frac{\mu_t}{\sigma_k}\right)\left(\frac{\partial k}{\partial x} + \frac{\partial k}{\partial y} + \frac{\partial k}{\partial z}\right)\right] \\ & + G - \rho\varepsilon\end{aligned} \tag{21}$$

ε-equation

$$\frac{\partial(\rho\varepsilon)}{\partial t}+\frac{\partial(\rho u\varepsilon)}{\partial x}+\frac{\partial(\rho v\varepsilon)}{\partial y}+\frac{\partial(\rho w\varepsilon)}{\partial z}=\frac{\partial}{\partial x}\left[\left(\mu+\frac{\mu_t}{\sigma_\varepsilon}\right)\left(\frac{\partial\varepsilon}{\partial x}+\frac{\partial\varepsilon}{\partial y}+\frac{\partial\varepsilon}{\partial z}\right)\right]+\frac{\partial}{\partial y}\left[\left(\mu+\frac{\mu_t}{\sigma_\varepsilon}\right)\left(\frac{\partial\varepsilon}{\partial x}+\frac{\partial\varepsilon}{\partial y}+\frac{\partial\varepsilon}{\partial z}\right)\right]+\frac{\partial}{\partial z}\left[\left(\mu+\frac{\mu_t}{\sigma_\varepsilon}\right)\left(\frac{\partial\varepsilon}{\partial x}+\frac{\partial\varepsilon}{\partial y}+\frac{\partial\varepsilon}{\partial z}\right)\right]+C_{\varepsilon 1}\frac{\varepsilon}{k}G-C_{\varepsilon 2}\rho\frac{\varepsilon^2}{k} \tag{22}$$

$$\mu_t=\rho C_u\frac{k^2}{\varepsilon} \tag{23}$$

$$G=2\mu_t E_{ij}E_{ij} \tag{24}$$

where, t: the time (s), u: Velocity field in the x-direction (m/s), v: Velocity field in the y-direction (m/s), w: Velocity field in the z-direction (m/s), ρ: the density in (kg/m^3), μ: the molecular viscosity coefficient (pa s), P: the correct pressure (pa), μ_t: the turbulent viscosity coefficient, which can be derived from the turbulent kinetic energy and turbulent dissipation rates ε, G: the turbulent kinetic energy source caused by the average velocity gradient defined by Eq. (23), E_{ij}: represents component of rate of deformation.

The model constants have the following default values [26, 27].

$$C_{\varepsilon 1}=1.44,\ C_{\varepsilon 2}=1.92,\ C_u=0.09,\ \sigma_k=1.0,\ \sigma_\varepsilon=1.3$$

To describe the changes of the free surface, VOF model defines a volume of fluid fraction function F = F(x, y, z, t) was considered. The compressibility of water and air flow within the weir were neglected.

4.2.2 Boundary Conditions

The boundary condition at the channel inlet is:

velocity inlet with V (0, 0) = Uo, water depth (0, 0) = (Yo) and VOF (water ratio fraction) = 1.

In the channel outlet, the boundary condition is:

Pressure outlet: P(L, y) = 0 and VOF (water ratio fraction) = 0.

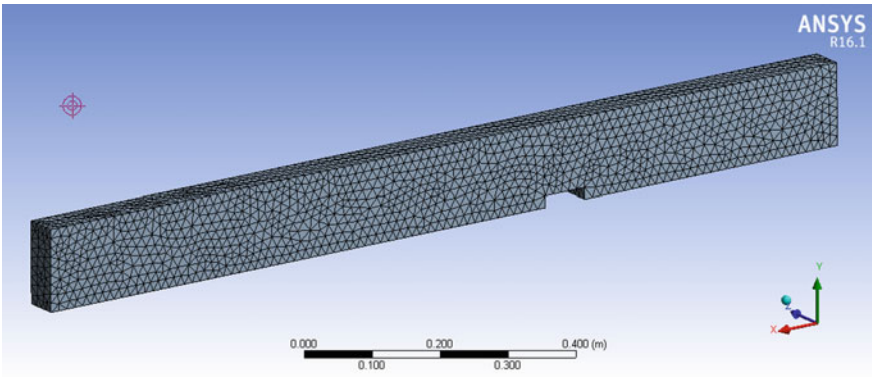

Fig. 7 Design of meshing model

The pressure condition is adopted, and the pressure value is the atmosphere pressure (1 atm). The side walls and floors of the weir and channel are set to no-slip wall boundary condition. Figure 7 and Tables 4 and 5 explain the geometry and

Table 4 Model geometry parts

Object name	Solid
State	Meshed
Graphics properties	
Visible	Yes
Transparency	1
Definition	
Suppressed	No
Coordinate system	Default coordinate system
Reference frame	Lagrangian
Material	
Fluid/solid	Defined by geometry (solid)
Bounding box	
Length X	1.4 m
Length Y	0.128 m
Length Z	5.1e−002 m
Properties	
Volume	9.0728e−003 m^3
Centroid X	0.70169 m
Centroid Y	6.4381e−002 m
Centroid Z	2.55e−002 m
Statistics	
Nodes	5639
Elements	25,304
Mesh metric	None

Table 5 Model meshing model

Object name	Mesh
State	Solved
Display	
Display style	Body color
Defaults	
Physics preference	CFD
Solver preference	Fluent
Relevance	100
Sizing	
Use advanced size function	On: curvature
Relevance center	Fine
Initial size seed	Active assembly
Smoothing	Medium
Transition	Slow
Span angle center	Fine
Curvature normal angle	Default (12.0°)
Min size	Default (1.4068e−004 m)
Max face size	Default (1.4068e−002 m)
Max size	Default (2.8135e−002 m)
Growth rate	Default (1.10)
Minimum edge length	1.8e−002 m
Inflation	
Use automatic inflation	None
Inflation option	Smooth transition
Transition ratio	0.272
Maximum layers	5
Growth rate	1.2
Inflation algorithm	Pre
View advanced options	No
Assembly meshing	
Method	None
Patch conforming options	
Triangle surface mesher	Program controlled
Patch independent options	
Topology checking	Yes
Advanced	
Number of CPUs for parallel part meshing	Program controlled
Shape checking	CFD
Element midside nodes	Dropped
Straight sided elements	
Number of retries	0

(continued)

Table 5 (continued)

Object name	Mesh
Extra retries for assembly	Yes
Rigid body behavior	Dimensionally reduced
Mesh morphing	Disabled
Defeaturing	
Pinch tolerance	Default (1.2661e−004 m)
Generate pinch on refresh	No
Automatic mesh based defeaturing	On
Defeaturing tolerance	Default (7.0338e−005 m)
Statistics	
Nodes	5639
Elements	25,304
Mesh metric	None

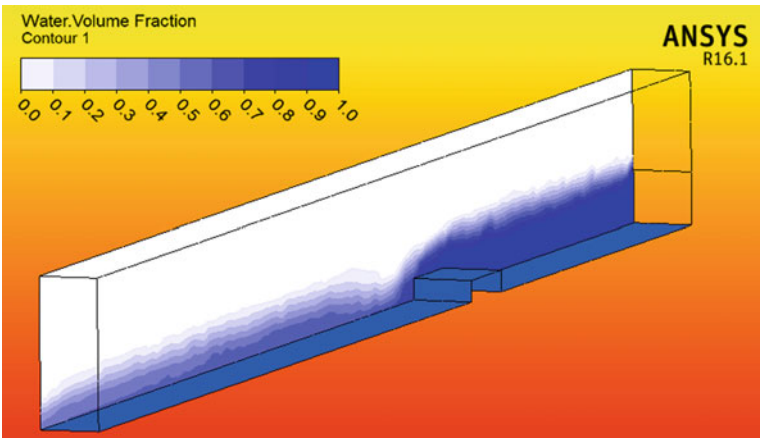

Fig. 8 Volume of fraction (VOF) simulated results

meshing properties of the CFD model for the case study of a horizontal slope with (Q_a = 0.171 L/s, inlet depth Y_o = 44 mm and Y_e = 7.3 mm). Figures 8 and 9 explain the water volume fraction and the stream flow pattern while Figs. 10 and 11 show the velocity distribution and the pressure distribution at the inlet and end edge sections. As the figures explain, the CFD model provides a very good simulation with all cases. The CFD model was also used to verify Eq. (11) for some elective experimental tests, see Table 6. The table indicates that the new formula provides a very good agreements results for all tests with a percentage error less than 10%.

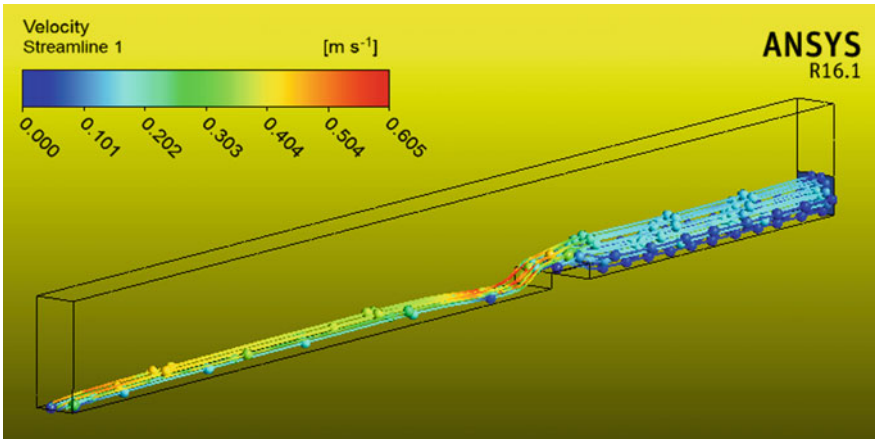

Fig. 9 Simulation of stream flow pattern

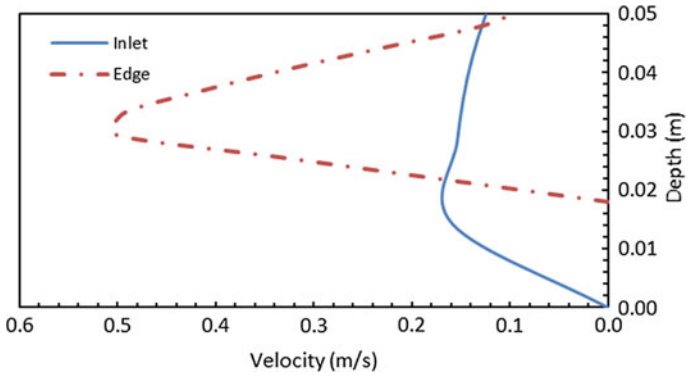

Fig. 10 Simulation results for the velocity distribution at the inlet and end edge sections

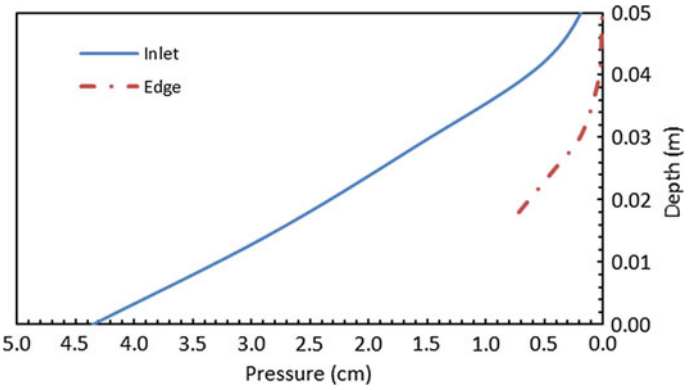

Fig. 11 Simulation results for the pressure distribution at the inlet and end edge sections

Table 6 Verification results of Eq. (11) with actual tests and simulated model

S_o	Q Actual (L/s)	Q Eq. (11) (L/s)	Q Simulation model (L/s)	Error % of Eq. (11) based on actual Q	Error % of Eq. (11) based on Q simulated
0.0000	0.1779	0.1757	0.186	1.26	5.54
0.0063	0.320	0.331	0.354	3.44	6.50
0.0225	0.500	0.488	0.477	2.40	2.31
0.028	0.490	0.473	0.446	3.47	6.05
0.0289	0.377	0.3901	0.402	3.47	2.96
0.0326	0.345	0.367	0.377	6.38	2.65
0.0333	0.510	0.532	0.524	4.31	1.53
0.035	0.433	0.456	0.467	5.31	2.36
0.0425	0.603	0.558	0.543	7.46	2.76
0.0495	0.4051	0.3967	0.387	2.07	2.51

5 Conclusions

The computational fluid dynamics (CFD) techniques considered as a very powerful tool to simulate different fluid dynamic problems. ANSYS FLUENT Ver. V.16.1 was used to simulate the flow over the sharp edge broad crested weir. A new flow rate estimation formula was derived depending on the relationship between the critical depth and the depth at the end edge section of the weir considering it as control section. For this purpose, ten experimental tests with several longitudinal slopes range from 0 to 0.0495 were achieved. The formula was statistically analyzed using several standard error indexes in order to investigate the confidence results of the formula. The statistical analyze indicates an excellent accuracy and a high confidence level for using the formula in flow rate estimation and with all cases. Furthermore, a CFD model was also designed and used to simulate the problem and to verify the formula for some elective experimental tests. The CFD model gave a very good simulation for flow pattern and VOF results with all cases. Also, the formula provides a very good agreements results with CFD model and the experimental tests with a percentage error less than 10%. The comparisons indicate that the CFD model could be considered as a very good tools to solve the complex hydraulic problems and predict the water surface profile in a high precise way.

Acknowledgements The authors would like to thank Mustansiriyah University (www.uomustansiriyah.edu.iq) Baghdad-Iraq for its support in the present work and the Hydraulic Laboratory staff in the College of Engineering for their support and helps with the experiments.

References

1. Amir HA, Rajaratnam N, David ZZ (2013) Discharge characteristics of weirs of finite crest length with upstream and downstream ramps. J Irrig Drain Eng 139:75–83
2. Ehsan G, Javad F, Naser S (2012) Flow characteristics of rectangular broad-crested weirs with sloped upstream face. J Hydrol Hydromech 60:87–100
3. Farzin S, Sanaz P, Ali HD, Davood FZ (2011) Discharge relations for rectangular broad-crested weirs. Tarim Bilim Derg J Agric Sci 17:324–336
4. Maghsoodi R, Mohammad SR, Hamed S, Hazi MA (2012) 3D-simulation of flow over submerged weirs. Int J Model Simul 32(4)
5. Hooman Hoseini S, Habib Musavi J, Sadegh Rafi V (2013) Determination of discharge coefficient of rectangular broad-crested side weir in trapezoidal channel by CFD. Int J Hydraul Eng 2(4):64–70
6. Samadi A, Arvanaghi H (2014) CFD simulation of flow over contracted compound arched rectangular sharp crested weirs. Int J Optim Civ Eng 4(4):549–560
7. Shaker AJ, Safa SI, Rondk AJ (2014) Surface roughness effects on discharge coefficient of broad crested weir. Res J Appl Sci Eng Technol 7(24):5227–5233
8. Seyed HH, Hossein A (2014) Flow over a broad-crested weir in subcritical flow conditions, physical study. J River Eng 2(1)
9. Sadiq SM (2014) Variation of discharge coefficient of spillway and broad crested weir due to the effective of the longitudinal slope in a non-horizontal channel. J Environ Sci Eng A 3(5):287–295
10. Ahmed S (2015) The coefficient of broad-crested weir in natural channels. Int J Sci Eng Inven (IJSEI) 1(1):1–13
11. Al-Hashimi SA, Madhloom H, Khalaf R, Nahi T, Al-Ansari N (2017) Flow over broad crested weirs: comparison of 2D and 3D models. J Civ Eng Archit 11:769–779
12. Sadiq SM, Al-Sharify ZT (2018) Experimental work and CFD model for flowrate estimating over OGEE spillway under longitudinal slope effect. Int J Civ Eng Technol (IJCIET) 9(13):430–439
13. Thulfikar RA, Abdul-Sahib TA, Zainab AN (2019) Laboratory experiments and numerical model of local scour around submerged sharp crested weirs. J King Saud Univ Eng Sci. https://doi.org/10.1016/j.jksues.2019.01.001
14. Chin DA (2006) Water resources engineering, 2nd edn. Prentice Hall
15. Chow VT (1986) Open-channel hydraulics. McGraw-Hill, New York, pp 365–380
16. Khurmi RS (2009) A textbook of hydraulic, fluid mechanics and hydraulic machines. Ram Nagar, New Delhi
17. Rajput RK (2008) A textbook of fluid mechanics and hydraulic machines. Ram Nagar, New Delhi
18. Sturm TW (2001) Open channel hydraulics. McGraw-Hill, New York
19. Subramanya K (1998) Flow in open channel. Tata McGraw Hill, New Delhi
20. Vennard K, Street L (1996) Elementary fluid mechanics. McGraw-Hill
21. Boiten W (2002) Flow measurement structures. Flow Meas Instrum 13:203–207
22. Soong TT (2004) Fundamentals of probability and statistics for engineers. Wiley, New York, USA
23. Aal GMA, Sobeah M, Helal E, El-Fooly M (2017) Improving energy dissipation on stepped spillways using breakers. Ain Shams Eng J. https://doi.org/10.1016/j.asej.2017.01.008
24. Al-Sharify ZT (2017) Flow and mixing of complex fluids. PhD thesis, University of Birmingham

25. Al-Sharify ZT, Zhao Y, Barigou M (2014) Comparing the performance of different impellers in mixing viscoplastic fluids: CFD, theory and experiment. In: The 5th Birmingham environment for academic research (BEAR) conference, Birmingham, UK
26. Ming-Liang Z, Yong-Ming S (2010) A 3D non-linear k–ε turbulent model for prediction of flow and mass transport in channel with vegetation. Appl Math Model 34(4):1021–1031
27. Mu Z, Zhang Z, Zao T (2012) Numerical simulation of 3-D flow field of spillway based on VOF method. Int Conf Mod Hydraul Eng Procedia Eng 28:808–812